Protumor steering of cancer inflammation by p50 nf-kb enhances colorectal cancer progression

Pro-tumor steering of cancer inflammation by p50 NF-κB enhances colorectal cancer progression

Chiara Porta[1], Alessandro Ippolito[1], Francesca Maria Consonni[1], Lorenzo Carraro[1], Giuseppe Celesti[2], Carmen Correale[2], Fabio Grizzi[2], Fabio Pasqualini[2], Silvia Tartari[2], Maurizio Rinaldi[1], Paolo Bianchi[2], Fiorella Balzac[3], Stefania Vetrano[2], Emilia Turco[3], Emilio Hirsch[3], Luigi Laghi[2], and Antonio Sica[1,2]

[1]Department of Pharmaceutical Sciences, Università del Piemonte Orientale "Amedeo Avogadro", Novara, Italy;

[2]Humanitas Clinical and Research Center, Rozzano, Italy;

[3]Department of Molecular Biotechnology and Health Sciences, Molecular Biotechnology Center, Torino, Italy

RUNNING TITLE: p50 NF-κB shapes CRC-promoting inflammation

KEYWORDS*:* macrophages, colorectal cancer, inflammation, NF-κB, cytokines

FUNDINGS: This work was supported by Ministero Universita` Ricerca, Italy (#20103FMJEN_003 and # RBAP11H2R9_005), Associazione Italiana Ricerca sul Cancro, Italy (N° 1558 and 19885), Ministero della Salute, Italy (129/GR-2011-02349580), Università del Piemonte Orientale (research funding 2016)

CORRESPONDING AUTHORS:

- Prof. Antonio Sica

Humanitas Clinical and Research Center,

via Manzoni 113, 20089 Rozzano, Italy

Department of Pharmaceutical Sciences

Università del Piemonte Orientale "A. Avogadro"

via Bovio 6, 28100 Novara, Italy

Phone: +39.02.8224.5111

Fax: +39.02.8224.5101

antonio.sica@humanitasresearch.it; antonio.sica@uniupo.it

- Chiara Porta PhD

Department of Pharmaceutical Sciences

Università del Piemonte Orientale "A. Avogadro"

via Bovio 6, 28100 Novara, Italy

phone: +39.0321.375883

fax: +39.0321.375821

e-mail: chiara.porta@uniupo.it

DISCLOSURE OF POTENTIAL CONFLICTS OF INTEREST:

The authors disclose no potential conflicts of interest.

Abstract

Although tumor-associated macrophages (TAMs) display a M2-skewed tumor-promoting phenotype in most cancers, in colorectal cancer (CRC), both TAM polarization and its impact remain controversial. We investigated the role of the M2-polarizing p50 NF-κB subunit in orchestrating TAM phenotype, tumor microenvironment composition, and CRC progression. We first demonstrated, by parallel studies in colitis-associated cancer (CAC) and in genetically driven Apc^{Min} mouse models, that the p50-dependent inhibition of M1-polarized gut inflammation supported CRC development. In accordance with these studies, $p50^{-/-}$ mice displayed exacerbated CAC with fewer and smaller tumors, along with enhanced levels of M1/Th1 cytokines/chemokines, including IL12 and CXCL10, whose administration restrained CAC development *in vivo*. The inflammatory profile supporting tumor resistance in colons from $p50^{-/-}$ tumor bearers correlated inversely with TAM load and positively with both recruitment of NK, NKT, $CD8^+$ T cells and number of apoptotic tumor cells. In agreement, myeloid-specific ablation of p50 promoted tumor resistance in mice, whereas in CRC patients, a high number of $p50^+$ TAMs at the invasive margin was associated with decreased *IL12A* and *TBX21* expression and worse post-surgical outcome. Our findings point to p50 involvement in CRC development, through its engagement in the pro-tumor activation of macrophages, and identify a candidate for prognostic and target therapeutic intervention.

Introduction

Colorectal cancer (CRC) development in inflammatory bowel disease patients is almost three-fold higher than the general population, making inflammation the third most common CRC risk factor after the hereditary CRC syndromes, familial

adenomatous polyposis coli and hereditary non-polyposis colon cancer (1). Even in sporadic and familial CRC tumors, a "smoldering inflammation" is present despite the lack of an obvious pre-existing inflammation (2,3). As a predominant immune population infiltrating the tumor, macrophages exert a pivotal role in the orchestration of cancer inflammation (4), by triggering either M1 or M2 activation states in response to microenvironmental signals (5). Selected pathways and transcription factors have been described to control the polarization state of macrophages (6). Among these, the transcription factor NF-κB is a key regulator of gut inflammation and functions, and aberrant activation of NF-κB has been frequently observed in human CRC, correlating with worse outcome. A IKKβ-dependent activation of NF-κB supports CRC cells proliferation, survival and epithelial-mesenchymal transition (7,8), as well as the expression of the tumor promoting cytokine IL6 by myeloid cells. In turn, NF-κB activates additional pathways of cancer cells proliferation and survival (e.g. STAT3) (9,10). Interestingly, IKKα ablation promoted IKKβ-driven NF-κB activation in intestinal epithelial cells and the subsequent recruitment of M1-polarized antitumor myeloid cells (11). However, despite this promising premise, targeting NF-κB remains a major challenge in CRC therapy, as its systemic inhibition leads to severe adverse effects (12).

Tumor-infiltrating leukocytes may exert beneficial or detrimental activities, depending on their functional state (13). Experimental and clinical studies indicate that the immunoscore, defined by type, density, and location of T cells, is an important prognostic factor in CRC, which has been suggested to overcome AJCC/UICC TNM classification, although this point remains debated (14,15). Tumor-associated macrophages (TAMs) (13,16) largely express an M2-skewed phenotype, associated with suppression of adaptive immune functions and promotion of angiogenesis and invasion (13). Accordingly, a high number of TAMs has been associated with poor prognosis in

several human cancers (17-19). However, TAMs can also express antitumor activities (20), and their role in CRC remains controversial (21-23). In CRC intratumoral macrophages appear to play tumor-promoting roles (24), whereas those located at the invasive front exert beneficial activities (25). Although the tumor microenvironment sculpts the phenotype of TAMs (13), the pathways driving their responses in the inner vs. peripheral tumor remain unknown. M1 and M2 macrophage populations are dynamically recruited and functionally modulated during CRC development in mice (26), and simultaneous accumulation of M1 (e.g. $NOS2^+$) and M2 (e.g. $CD163^+$) and mixed macrophage populations are observed in human CRC tumors (27). The molecular basis and the clinical relevance of this dynamic reprogramming and heterogeneity of TAMs are still unclear. We have reported that progressive nuclear accumulation of p50 NF-κB in macrophages promotes tolerance and M2-polarized activation (28,29). Based on this evidence, we investigated the impact of p50 NF-κB-driven inflammation in CRC development and progression.

Materials and methods

Patients: The study was approved by the Institute Ethical Committee, and written informed consent was obtained from patients. The study was conducted on 47 specimens of primary tumor from a well-studied, consecutive series of patients resected for stage II/III CRC at the Humanitas Research Hospital between 1997 and 2006, for which both frozen tissues and paraffin embedded specimens were available (30). Patients who had received neoadjuvant radio-chemotherapy were excluded from the study. Patient demographics and clinical and pathological features (Supplementary Table S1) were available at the hospital intranet system, which also was used for retrieving clinical data concerning patients' post-surgical outcome.

Mice: C57BL/6J wildtype (wt) mice (Charles Rivers laboratories), p50 NF-κB-deficient mice (28), originally donated by Drs. Michael Karin and Giuseppina Bonizzi (University of California at San Diego Medical School),_Apc^{Min} mice (Jackson Laboratories Bar Harbor, Maine, USA) were on the same C57BL/6J background. The Apc^{Min} mice were crossed with p50$^{-/-}$ mice in order to generate Apc^{Min}p50$^{-/-}$ mice. Mice carrying the NFKB1 floxed allele (p50$^{Fl/Fl}$ mice) were generated as described below.

The targeting construct to generate a NFKB1flox/flox (p50$^{Fl/Fl}$) mice was designed as follows: the eighth exon of NFKB1 gene was flanked with loxP sites, and the neomycin resistance gene, flanked with Flippase Recognition Target (FRT) sites to permit its excision, was inserted in the seventh intron. This construct was introduced by electroporation into mouse ES cells. Homologous recombination was confirmed by southern blot and ES cells carrying NFKB1fl-neo allele were injected into C57 blastocysts to generate germ-line chimeras. The neomycin resistance cassette in the targeting construct was removed by crossing heterozygous NFKB1Fl/+-neo mice with C57BL6 mice carrying the FLP recombinase under the control of the actin promoter (kindly provided by Dr. Rolf Sprengel) to produce mice carrying the NFKB1 floxed allele (p50$^{Fl/+}$ mice). p50$^{Fl/Fl}$ mice were crossed with B6.129P2-Lyz2tm1(cre)Ifo/J and B6.Cg-Tg(Vil1-cre) mice (Jackson Laboratories, Bar Harbor, Maine, USA) to generate p50$^{Fl/Fl}$;Lyz2Cre and p50$^{Fl/Fl}$;VillinCre mice, respectively. Genotyping of mice was performed by PCR using the following primers: p50FloxF1: 5'-CTGGGCTCCTAGCGGGGGAG-3' and p50FloxR1, 5'- GGCTGACATGTGGGTCCTCAGC-3', which gave rise to an amplicon of 282 bp for the floxed allele and of 182bp for the wt allele. To detect Lyz2Cre and VillinCre transgenes, we adopted the PCR protocols provided by Jackson laboratories.

To confirm p50 NF-κB ablation in myeloid cells ($p50^{Fl/Fl}$;Lyz2Cre mice) and enterocytes ($p50^{Fl/Fl}$;VillinCre mice), thioglycolate-elicited peritoneal macrophages from $p50^{Fl/Fl}$;Lyz2Cre mice and littermate controls ($p50^{Fl/Fl}$ mice) were analyzed for p50 expression by western blot as previously described (28)(Supplementary Fig. S1A). Sections of formalin-fixed, paraffin-embedded colons from $p50^{Fl/Fl}$;VillinCre mice and littermate controls ($p50^{Fl/Fl}$ mice) were evaluated for p50 expression by immunohistochemistry with rabbit monoclonal anti-p50 (clone E381; Abcam) (Supplementary Fig. S1B). Detailed information is provided below (see "Immunohistochemistry or immunofluorescence" section).

The study was designed in compliance with principles set out in the following laws, regulations, and policies governing the care and use of laboratory animals: Italian Governing Law (Legislative Decree 116 of Jan. 27, 1992); EU directives and guidelines (EEC Council Directive 86/609, OJ L 358, 12/12/1986); Legislative Decree September 19, 1994, n. 626 (89/391/CEE, 89/654/CEE, 89/655/CEE, 89/656/CEE, 90/269/CEE, 90/270/CEE, 90/394/CEE, 90/679/CEE); the NIH Guide for the Care and Use of Laboratory Animals (1996 edition), and it was approved by the scientific board of Humanitas Clinical and Research Center. In all experiments, sex- and age-matched mice bred in the same specific-pathogen-free (SPF) animal facility were used. Mice were monitored daily and euthanized when displaying excessive discomfort. To assess overall survival, Apc^{Min} and $Apc^{Min}p50^{-/-}$ mice were continuously monitored for a period of up to 40 weeks.

Azoxymethane (AOM)/ DSS-induced colorectal cancer: 6-8 weeks old mice (wt and $p50^{-/-}$, $p50^{Fl/Fl}$;Lyz2Cre and $p50^{Fl/Fl}$ littermates, and $p50^{Fl/Fl}$;VillinCre and $p50^{Fl/Fl}$ littermates) and 16-week old mice (wt and $p50^{-/-}$ mice that were subjected to bone

marrow transplantation at 8 weeks of age) were injected intraperitoneally (i.p.) with a single dose (10 mg/kg of body weight) of the mutagenic agent azoxymethane (Sigma). 5 days later, mice received water with 2% dextran sodium sulfate (DSS) (MP Biomedicals molecular mass; 40 kDa) over 5 days, followed by 16 days of regular water. This cycle of DSS treatment was repeated two more times, and mice were sacrificed 3 weeks after the last cycle (31). The clinical course of colitis was evaluated by monitoring mice body weight during the course of the experiment and by measuring colon length at necroscopy. At the time of harvest, mice were euthanized, colons were resected, flushed with saline solution, opened longitudinally and macroscopically evaluated for tumors number. This protocol was used in all the experiments unless otherwise specified.

When specified, starting from day 15 (e.g. recovery phase of the first DSS cycle), wt mice underwent i.p. administration of 100 ng IL12 (Biolegend) diluted in 100 µL of 1% BSA phosphate-buffered saline (PBS) solution or intra-rectal injection of 500 ng CXCL10 (Biolegend), once a week. For CXCL10 treatment, mice were anesthetized by i.p. injection of Ketamina (Imalgene; 100 mg/kg) and Xilazina (Rompun; 10 mg/kg). Next, 500 ng of CXCL10 (Biolegend) diluted in 50 µL of 1% BSA PBS solution was rectally administered via a flexible plastic feeding tube inserted 3 cm proximally to the anus. After rectal administration, mice were kept in an inverted position for 30 seconds. As controls, mice received vehicle only.

When specified, starting from the day before the first DSS treatment, wt and $p50^{-/-}$ mice received an i.p. injection of 0.3 mg anti-mouse CD4 (clone GK1.5; BioXcell) and 0.3 mg anti-mouse CD8 (clone 2.43; BioXcell), once a week for the entire experimental period. FACS analysis of peripheral blood samples confirmed $CD4^+$ and $CD8^+$ cells depletion for 7 days.

Histological analysis: At the end of AOM/DSS experiments, mice were euthanized, colons were resected, flushed with PBS, opened longitudinally and rolled up. At the indicated age, Apc^{Min} and $Apc^{Min}p50^{-/-}$ mice were euthanized. Both small gut and colons were harvested, flushed with PBS, and prepared according to swiss and roll technique. Gut samples were fixed in 10% neutral buffered formalin for 24 hours and paraffin-embedded. 4 µm of serial tissue sections were stained with hematoxylin and eosin staining (H&E) and analyzed in a blinded fashion by a pathologist. Histological evaluation of grade of colitis was performed according to the score of Cooper et al. (32), and Suzuki et al. (33), only slightly modified to adapt it to the findings of present study. 0= Normal colonic mucosa, 1= Shortening and loss of the basal one-third of the crypts with mild inflammation in the mucosa, 2= Loss of the basal two-thirds of the crypts with moderate inflammation in the mucosa, occasionally extending into submucosa, 3= Loss of the entire crypts with severe inflammation in the mucosa and submucosa but with the retainment of the surface epithelium, 4= Presence of mucosal ulcer with severe inflammation in the mucosa, submucosa, submucosa, tunica muscularis, and/or subserosa. The scoring of colitis was made at 40x magnification on the entire colon swiss roll with or without proliferative lesions and expressed as mean score/mouse. Additionally, the number of ulcers, and total number and size of the neoplastic lesions was recorded.

Bone-marrow transfer. Bone marrow (BM) cells were flushed from femurs and tibia of CD45.1 wt or $p50^{-/-}$ mice. Recipient $CD45.2^{+}p50^{-/-}$ or wt mice were lethally irradiated (900 cGy). 5 hours later, $5x10^{6}$ red blood cell-depleted BM cells were injected intravenously in recipient mice. BM reconstitution was evaluated 6 weeks after transplantation by flow cytometry on peripheral blood.

Analysis of p50 nuclear accumulation in murine and human TAMs: Mouse colonic sections (untreated and AOM/DSS-treated wt mice) of 10 μm thickness and CRC specimens of 3 μm thickness were deparaffinized and rehydrated. Human slides were exposed to UV radiation overnight. Antigen unmasking was carried out by incubation in a decloaker chamber at 125°C for 3 minutes and 90°C for 10 minutes in Diva Decloaker retrieval solution (Biocare). Unspecific binding sites were blocked with 2% BSA, 0.1% Triton X-100 in 0.05% Tween 20 phosphate buffer solution (PBST) for 1 hour at room temperature. Next, murine samples were stained at room temperature in a humidified chamber with mouse monoclonal anti-p65 NF-κB (clone L8F6; Cell Signaling; 1/100 dilution in PBST) for 1 hour and then incubated with rabbit monoclonal anti-p50 NF-κB (clone E381; Abcam; 1/250 dilution in PBST) for 4 hours. Samples were then incubated with rat monoclonal anti-mouse F4/80 (clone CI:A3-1; AbD Serotec; 1/100 diluted in PBST) for 1 hour. After each staining, slides were washed with PBST. Next, goat anti-mouse Alexa Fluor 555-conjugated (Cat. # A28180; Thermofisher), goat anti-rabbit Alexa Fluor 647-conjugated (Cat. # A27040; Thermofisher), and goat anti-rat Alexa Fluor488-conjugated (Cat. # A-11006; Thermofisher) (1/1000 dilution in PBST) were incubated for 1 hour at room temperature in humidified chamber. Human samples were stained at room temperature in a humidified chamber with mouse monoclonal anti-human CD68 (clone M0814; Dako; 1/200 dilution in PBST) for 1 hour, followed by rabbit monoclonal anti-p50 NF-κB (clone E381; Abcam; 1/250 dilution in PBST) for 4 hours. After each staining, slides were washed with PBST, followed by addition of goat anti-mouse Alexa Fluor 488-conjugated and goat anti-rabbit Alexa Fluor 647-conjugated (both diluted 1/1000 in PBST) and incubated for 1 hour at room temperature in a humidified chamber. Nuclei were stained with DAPI (Life Technologies) and then

mounted with ProLong Antifade Gold Reagent (Life Technologies). Slides were analyzed with Olympus Fluorview FV1000 confocal microscope with 60X (N.A.0.4), and single-cell count was performed by lab personnel under the supervision of imaging core facility personnel (n≥8 field for every sample; n≥3 for every condition).

Real-Time PCR Analysis: At the end of AOM/DSS treatment, colons from wt and $p50^{-/-}$ mice were washed with ice-cold PBS, and then macroscopic tumors and the adjacent healthy tissue were harvested and maintained in RNA stabilization solution (RNAlater, Ambion). Similarly, colons were collected from untreated wt and $p50^{-/-}$ mice and from AOM/DSS-treated wt mice 9 days after the beginning of first cycle of DSS treatment. Similarly, macroscopic colonic tumors and the adjacent healthy tissue were harvested from 20-24-week old Apc^{Min} and $Apc^{Min}p50^{-/-}$ mice. Total RNA was extracted from mouse tissues using the TissueLyser II (Qiagen) and RNeasy Lipid Tissue Mini Kit (Qiagen) and from human fresh stage II and III CRC surgical specimens by using TRIzol® Reagent (Thermo Fisher Scientific), according to manufacturer's instructions. RNA quality was assessed as 260/280 and 260/230 OD ratio >1.5. 1 μg of RNA was reverse transcribed by the cDNA Archive kit (Applied Biosystems), and then 20 ng of template was amplified using GOTAQ qPCR Master Mix (Promega) and detected by the CFX96 Real-Time System (Biorad). All samples were run in triplicate. Expression data were normalized to Actin or 18S mRNA expression and were analyzed by the $2^{-\Delta\Delta Ct}$ method. Results are expressed as fold upregulation with respect to the control cell population specified in the figure legend. The sequences of gene-specific primers were obtained from previous published papers (10,29,34), or were designed by using https://www.ncbi.nlm.nih.gov/tools/primer-blast/. The primers are synthetized by Invitrogen and are reported in Supplementary Table S2.

Immunohistochemistry or immunofluorescence: Formalin-fixed, paraffin-embedded colons from untreated and AOM/DSS-treated mice (wt and $p50^{-/-}$), as well as from $p50^{Fl/Fl}$ and $p50^{Fl/Fl}$;VillinCre mice, were cut in sections of 10 μm thickness. Colonic slides were deparaffinized and rehydrated. Antigen unmasking was carried out by incubation in a decloaker chamber at 125°C for 3 minutes and 90°C for 10 minutes in Diva Decloaker retrieval solution (Biocare Medical, USA). Endogenous peroxidases were blocked with Peroxidized 1 (Biocare Medical, USA) for 20 min, then unspecific binding sites were blocked with 2% BSA PBS at room temperature for 1 hour.

Immunohistochemistry was performed at room temperature: rat anti-mouse F4/80 (clone CI:A3-1; AbD Serotec; 1/100 dilution in PBST) for 1 hour; rat anti-mouse Ly6G (clone 1A8; BD Bioscences; 1/200 dilution in PBST) for 1 hour; rat anti-mouse Ly6C (clone ER-MP20; ThermoFisher; 1/100 dilution in PBST) for1 hour; rabbit polyclonal anti-human CD3 (cat. #A0452; DAKO; 1/100 dilution in PBST) for 1 hour; rabbit polyclonal antibody against cleaved-caspase 3 antigen (cat. #Asp175; Cell Signaling; 1/200 dilution in PBST) for 1 hour; and rabbit monoclonal anti-p50 NF-κB (clone E381; Abcam; 1/250 dilution in PBST) for 1 hour. MACH1 Universal HRP Polymer (Biocare Medical, USA) was used as secondary antibody for 30 min. The reaction was developed with 3,3'-Diaminobenzidine (DAB), and nuclei were counterstained with hematoxylin and then mounted with Eukitt. The total antigen$^+$ area (μm^2) and fraction area (total antigen$^+$ area/total area of field at 200x) were evaluated by lab personnel under the supervision of imaging core facility personnel using the ImageJ analysis program (http://rsb.info.nih.gov/ij/) in 200x microscopic fields selected within the neoplastic lesions ("tumor") and the adjacent non-neoplastic mucosa ("non-tumor").

Colons from untreated and AOM/DSS-treated mice (wt and $p50^{-/-}$) were frozen in OCT, and then sections were cut at 8 μm thickness. Colonic slides were fixed for 3 min in

cold acetone:chloroform (3:1), followed by incubated with 5% Donkey Serum, 2% BSA, 0.1% Triton X-100, 0.2% NP-40, PBST solution for 1h at room temperature to block unspecific binding sites.

Immunofluorescence staining was carried out at room temperature in humidified chamber with polyclonal rabbit anti-human CD3 (cat. #A0452; DAKO; 1/100 dilution) for 1 hour and polyclonal goat anti-mouse NKp46 (cat. #AF2225; R&D; 1/100 dilution) for 1 hour. After being washed with PBST, slides were incubated at room temperature in humidified chamber for 1 hour with donkey anti-goat Alexa Fluor 488-conjugated and goat anti-rabbit Alexa Fluor 647-conjugated (both 1/1000 dilution) in PBST. Nuclei were stained with DAPI (Life Technologies) and then mounted with ProLong Antifade Gold Reagent (Life Technologies). Slides were analyzed by lab personnel under the supervision of imaging core facility personnel using an Olympus Fluoview FV1000 laser scanning confocal microscope with 60X (N.A.0.4), and single-cell count was performed (n≥5 field for every sample; n≥3 for every condition).

Fluorescence-activated cell sorting (FACS) analysis: Colons harvested from AOM/DSS-treated and untreated mice (wt and $p50^{-/-}$) were longitudinally cut and washed with PBS to remove feces and debris. Tumors and tumor-free colon tissues were cut in 0.5 cm pieces and incubated under rotation in HBSS containing 5% FBS, 10 mM HEPES, 2.5 mM EDTA for 20 minutes at 37°C (twice). Tissues were then finely minced and incubated under rotation in HBSS containing 5% FBS, 10 mM HEPES, dispase/collagenase (1mg/mL; Roche), collagenase IV (250 μg/mL; Serva), and DNAse (40 μg/mL; Roche) for 20 minutes at 37°C. Single-cell suspensions were sequentially filtered through a 100 μm and 70 μm cell strainers and centrifuged 10 minutes at 1300 rpm. Cells were incubated with TruStain fcX™ (anti-CD16/32) antibody (Biolegend),

according to the manufacturer's instructions. Afterwards 0.5-1x10^6 cells were stained with antigen-specific antibodies in the presence of LIVE/DEAD Fixable Violet (Invitrogen) to evaluate cell viability. Cells were stained in 0.5% FBS, HBSS solution with: anti-CD45–FITC or -PerCP (clone 30-F11), CD11b–PerCP or -APC (clone M1/70), F4/80–PE-Cy7 or -PE (clone BM8), Ly6C-PE (clone HK1.4), NK1.1-APC (clone PK136), CD4–PE-Cy7 (clone GK1.5), CD8-APC (clone 53-6.7), CD3-PE (clone 145-2C11), TNFα-APC (clone MP6-XT22), IL12–PE-Cy7 (clone C15.6), IFNγ-FITC (clone XMG1.2) (all from Biolegend), unconjugated polyclonal rabbit anti-mouse NOS2 (Abcam) followed by incubation with secondary goat anti-rabbit Alexa Fluor 488-conjugated (Invitrogen, Molecular Probes, Carlsbad, CA).

Cytofix/Cytoperm and Permwash staining kit (BD Pharmigen) were used for intracellular staining (TNFα, IL12, IFNγ, iNOS), according to the manufacturer's instructions. Expression levels of cytokines (IL12, TNFα, IFNγ) were evaluated after 3 hours of stimulation with pherbol-12 13-acetate (PMA; 40ng/mL) and ionomycin (1 μg/mL) in presence of brefeldin A (5 μg/mL; Sigma). Cells were acquired using FACSCanto II or LSR Fortessa (BD Bioscience), and data were analyzed using 9.3.2 FlowJo software (Treestar). Mean fluorescence intensity (MFI) was normalized to isotype control or fluorescence minus one controls.

Statistical analysis: Data are expressed as mean ± SEM. Statistical significance between two groups was assessed by unpaired, one- or two-tailed Student *t* test or Mann Whitney test, and multiple groups were analyzed by Kruskal-Wallis test or one-way ANOVA (GraphPad Prism software). $P \leq 0.05$ was considered significant.

The mean percentage (GraphPad Prism software) of $p50^+$ TAMs associated to the occurrence of post-surgical metastasis was used to divide patients with high (above

mean) and low numbers of $p50^+$ TAMs used in Kaplan-Meier curves for disease-free survival (DFS) and CRC-specific survival (CRC-SS). *P* values were calculated by log-rank test. Receiver operating characteristic (ROC) curves were used to determine cut-off values for the investigated transcripts associated to the occurrence of post-surgical progression. These cut-offs were used to divide patients with high and low mRNA expression in Kaplan-Meir curves.

RESULTS

Colitis-associated cancer development is paralleled by M2 polarization

Whereas type 1 immune responses restrain CRC progression (35), the molecular events driving the balance between antitumor and tumor-promoting inflammation in CRC remain unclear. We first addressed this issue in a chemical model of colitis-associated CRC (CAC) (31). We analyzed the mRNA expression of relevant inflammatory genes in colons from wt mice, obtained 9 days (colitis) and 80-90 days (established tumor development) after the first DSS administration.

As compared to control colons, we identified a gene cluster (gene cluster 1) that was similarly upregulated in both phases, colitis and tumor, whereas a second cluster of genes (cluster 2) was more expressed in established tumors (Fig. 1A). Other genes tested included *Ptgs2,* which was more expressed in tumors compared to control colons, and *ArgI*, which was more expressed in tumors than colitis. An increased expression of *Ccl5* was observed in colitis rather than in tumors, and *Il12a, Prf1, Gzmb, Fasl,* and *Il21* were not significantly upregulated in both colitis and tumors (Supplementary Fig. S2). In the healthy mucosa, adjacent to the excised tumor lesions, expression of both gene clusters was comparable to those observed in the colon of untreated control mice (Fig. 1A). The higher expression of cluster 2 in tumor tissues, containing the tumor promoting

genes *Tnf* and *Il23a* (3), along with markers of Th2/M2 polarized inflammation (*Il10, Tgfb1, Ccl17, Ccl22*) (36) (Fig. 1A), represented a tumor-promoting activity. In contrast, cluster 1 was comprised of genes associated with an antitumor Th1/M1-skewed immune profile (*Il1b, Il6, Il12b, Il27, Ebi3, Cxcl9, Cxcl10, Nos2, Ifng*) (Fig. 1A)(35). These results indicate that a shift in the polarized inflammatory response from type 1 to type 2 occurred during the transition from colitis to cancer.

To investigate the molecular basis of this transcriptional reprogramming, we focused on macrophages. Because nuclear accumulation of p50 in macrophages promotes an M2-like transcriptional program (28,29), we analyzed the nuclear levels of the p50 and p65 NF-κB subunits, in both lamina propria macrophages and TAMs. Confocal microscopy showed a selective accumulation of nuclear p50 over p65 in TAMs compared to lamina propria macrophages from control mice (Fig. 1B). These results indicate that the tumor-promoting reprogramming of CRC-associated inflammation occurred during tumor development, in conjunction with nuclear accumulation of p50 NF-κB in TAMs.

p50 NF-κB deficiency restrains CAC development

To investigate the impact of p50 NF-κB ablation in the inflammatory reprogramming supporting CAC development, wt and $p50^{-/-}$ mice were treated with AOM/DSS. We initially examined the inflammatory response developed by wt and $p50^{-/-}$ mice after a single round of DSS. No differences in colon length were observed between wt and $p50^{-/-}$ control mice drinking untreated water (Supplementary Fig. S3B, right), whereas with DSS treatment, lack of p50 resulted in a higher mortality rate (Supplementary Fig. S3A), severe body weight loss (Supplementary Fig. S3B, left), and colon shortening (Supplementary Fig. S3B, right), indicating that the p50 NF-κB subunit

is an essential regulator of chemically induced intestinal inflammation.

To examine the role of p50 NF-κB in CAC, wt and $p50^{-/-}$ mice were treated with AOM in combination with three rounds of DSS treatment. In keeping with the acute model of colitis, lack of p50 resulted in increased weight loss (Fig. 2A, top) and a higher degree of intestinal inflammation, in both number of ulcers in colon tissues and colitis score, over the entire experimental period (Fig. 2A, middle). Compared to wt mice, at necropsy, $p50^{-/-}$ mice showed a significant decrease in colon length (Fig. 2A, bottom). Conversely, compared to wt mice, both macroscopic and histological analysis of $p50^{-/-}$ colons showed a significant decrease in the number of neoplastic lesions, together with reduced size (Fig. 2B). Collectively, these results indicate a tumor-promoting role for p50-driven inflammation in CAC development.

Hence, we examined the expression of genes belonging to clusters 1 and 2 (Fig. 1A) in the tumor-resistant, p50-deficient mice. Compared to their wt counterpart, we observed a strong inhibition of *Il23a* expression in tumors, paralleled by a significant upregulation of Th1/M1 inflammatory genes (*Il12b, Il27, Ebi3, Cxcl9, Cxcl10, Nos2, Ifng)* (Fig. 2C, top). Consistently, the lack of p50 also resulted in higher expression of *Prf1, GzbB, Fasl, Il21, Ccl5*_(Fig. 2C, bottom). FACS analysis of tumor immune infiltrates confirmed that genetic ablation of p50 in TAMs enhanced expression of M1-related gene products (e.g. TNFα, IL12, iNOS) (Fig. 2D, top), along with increased frequency of IFNγ expressing $CD8^+$ and $CD4^+$ T cells (Fig. 2D bottom). These results indicate that boosting of CAC development by p50 was paralleled by its ability to restrain Th1/M1 immune responses.

To strengthen the association between antitumor resistance and gene cluster 1, AOM/DSS-treated mice underwent systemic (intraperitoneal) or local (intra-rectal) administration of selected Th1/M1 cytokines/chemokines, IL12 (100 ng) and CXCL10

(500 ng), once a week (Fig. 3A). Despite a similar body weight loss (Fig. 3B) and colon length (Fig. 3C) in the untreated and treated groups, both IL12 and CXCL10 induced a significant reduction in tumor multiplicity (Fig. 3D), confirming the antitumor activity of the Th1/M1-polarized immune response.

Because the molecular determinants of intestinal carcinogenesis may differ in models of CAC compared to genetically driven CRCs (37,38), we evaluated the role of p50 NF-κB in the Apc^{Min} mouse model of spontaneous intestinal carcinogenesis (39). To this aim, Apc^{Min} and $p50^{-/-}$ mice were crossed to generate double $Apc^{Min}p50^{-/-}$ mice. Subsequently, small intestines and colons were harvested from both Apc^{Min} and $Apc^{Min}p50^{-/-}$ mice at different time points (12 and 18 weeks) and were analyzed for the number of tumor lesions. As expected, tumor multiplicity and size increased over time. However, compared to Apc^{Min} mice, a significant inhibition of both tumor incidence and growth was observed in the $Apc^{Min}p50^{-/-}$ group (Fig. 4A), which was associated with increased survival from 6 (mean 22 weeks) to 10 months (mean 41 weeks) (Fig. 4B).

We then investigated whether the inflammatory response detected in the CAC tumor model was also activated in the Apc^{Min} mice. Because Apc^{Min} mice largely develop tumors in the small intestine, CRC lesions were obtained from the colon of 23-week old mice, when tumors arise also in the large intestine. Similar to the CAC model, most of the genes belonging to clusters 1 and 2 were upregulated in tumor tissues compared to the adjacent healthy mucosa (Fig. 4C), whereas lack of p50 confirmed the selective reduction in the tumor-promoting *Il23a* gene transcript, along with the enhanced expression of Th1/M1 genes (Fig. 4D). The results obtained in both the CAC and the Apc^{Min} models indicate that, irrespective of the etiological events, p50 promotes intestinal cancer development by hampering Th1/M1-dependent antitumor responses.

To gain additional insights in the p50-driven M2 reprogramming of TAMs, we

adopted the immunogenic MC38 transplantable CRC model, characterized by an abundant TAM infiltrate (40). As expected, tumor growth was significantly inhibited in $p50^{-/-}$ mice (Supplementary Fig. S4A). Compared to the wt counterparts, TAMs purified from $p50^{-/-}$ mice by magnetic cell sorting (Supplementary Fig. S4B) displayed enhanced mRNA expression of selected M1 genes (*Cxcl9*, *Il12b*, *Ifng*, *Il1b*, *Tnf* and *Il23a*) (Supplementary Fig. S4C), along with increased protein levels of TNFα and CXCL9 (Supplementary Fig. S4D). Consistent with the tumor-promoting activity of p50-driven, M2-polarized activation, co-injection of magnetically sorted wt TAMs significantly enhanced the growth of the MC38 tumors in p50-deficient mice compared to co-injection of $p50^{-/-}$ TAMs (Supplementary Fig. S4E).

Lack of p50 restrains TAM accumulation and favors T-cell infiltration

Taken together, data from the preclinical models indicate that p50 NF-κB impairs antitumor immunity. Hence, we investigated the composition of the immune infiltrate in untreated and AOM/DSS-treated conditions, in both wt and p50-deficient mice. No changes were observed in the number of tumor and lamina propria neutrophils ($Ly6G^+$ cells), whereas lack of p50 resulted in reduced tumor and lamina propria monocytes ($Ly6C^+$ cells) and macrophages ($F4/80^+$ cells) and an increased number of T lymphocytes ($CD3^+$ cells), NK ($NKp46^+CD3^-$), and NKT ($NKp46^+CD3^+$) cells in both tumors and adjacent healthy tissues (Fig. 5A and B, Supplementary Fig. S5A and B). Supplementary Fig. S6 shows that in the absence of p50, the number of mucosal monocytes ($Ly6C^+$) and macrophages ($F4/80^+$) were significantly reduced, even in untreated mice, whereas colonic NK, NKT, and T cells were unaffected. FACS analysis of CRC lesions isolated from AOM/DSS-treated mice further confirmed that p50 deficiency impairs TAM accumulation, while increasing the frequency of lymphoid effector cells

(NK, NKT, $CD8^+$ T cells) (Fig. 5C). This observation was corroborated through the expression analysis of genes encoding for lineage-specific markers, demonstrating that lack of p50 promotes an increased mRNA expression of both the *Cd8* and *Tbx21* (Tbet) genes, whereas the transcripts for Cd4 and the transcription factors Gata3, Rorc2 (RORγt), and Foxp3, respectively guiding differentiation of Th2/ILC2, Th17/ILC3, and Treg cells, did not change (Fig. 5D). These results further indicate that p50 NF-κB was involved in controlling the homing of lymphoid and myeloid cells to the gut and, hence, playing a crucial role in the control of intestinal innate and adaptive immune response. To assess the role of T cells in antitumor immunity consequent to p50 ablation, animals were next injected once a week with depleting anti-CD4 and anti-CD8 during the entire AOM/DSS treatment. Depletion of $CD4^+$ and $CD8^+$ T cells resulted in a consistent augmentation of tumor burden in p50 knockouts (Fig. 5E), confirming that p50 reduced both recruitment and antitumor activity of T cells.

Lack of p50 NF-κB impairs survival of colorectal cancer cells

Our data support the concept that the absence of p50 NF-κB increases cytotoxic immune functions, thus, preventing tumor multiplicity and growth. We then investigated colonic cancer cell proliferation and survival in wt and $p50^{-/-}$ mice. Colons were harvested from untreated and AOM/DSS treated mice and immunostained with anti-Ki67 and anti-active caspase-3. Although in both untreated and AOM/DSS-treated conditions, lack of p50 generated longer crypts with a higher proliferation rate of colonic epithelial cells, it did not affect cancer cell proliferation (Supplementary Fig. S7A). In accordance with this finding, p50 deficiency increased the expression of genes associated with cell cycle progression in the normal colonic mucosa from either untreated or AOM/DSS-treated mice, whereas no differences were found between wt

and $p50^{-/-}$ cancer cells (Supplementary Fig. S7B). Along with NF-κB, STAT3 is a key orchestrator of cell proliferation and survival, which is upregulated in AOM/DSS-induced CRC (9,10). Immunohistochemical analysis of wt and $p50^{-/-}$ colon tissues showed similar STAT3 phosphorylation between wt and $p50^{-/-}$ neoplastic cells (Supplementary Fig. S7C), suggesting that, in this context, p50 acts independently from STAT3. In contrast, colons from AOM/DSS-treated $p50^{-/-}$ mice displayed an increased number of cells expressing the activated form of caspase-3, indicating that absence of p50 impairs epithelial and cancer cell survival (Fig. 6A). Accordingly, tumors harvested from $p50^{-/-}$ mice expressed higher pro-apoptotic *Bak1* and lower pro-survival *Bcl2l1* (Fig. 6B), whereas no differences were found in the expression of *Bcl2* (anti-apoptotic), *Survivin* (anti-apoptotic), and *Bax* (pro-apoptotic) genes (Fig. 6B). No differences were detected in the number of apoptotic cells (Fig. 6A) and gene transcripts (Fig. 6B) between the colons of wt and $p50^{-/-}$ naïve mice. Overall these results indicate that inflammatory conditions arising in the absence of p50 impaired survival of both colonic epithelial and cancer cells.

Density of $p50^{+}$ TAMs is directly associated with a worse CRC patient outcome

To assess the role of p50 NF-κB in both macrophages and intestinal epithelial cells in CAC development, $p50^{-/-}$ and wt bone marrow (BM) cells were respectively transplanted in sublethally irradiated wt and $p50^{-/-}$ recipients. Compared to control mice (wt mice reconstituted with wt BM), only chimeric mice carrying hematopoietic-specific ablation of p50 displayed a tumor resistant phenotype in response to AOM/DSS treatment (Fig. 7A). We then generated mice carrying a specific ablation of p50 in myeloid cells ($p50^{Fl/Fl}$;Lyz2Cre) and in enterocytes ($p50^{Fl/Fl}$;VillinCre). Following AOM/DSS treatment, $p50^{Fl/Fl}$;Lyz2Cre mice developed less CRC lesions than littermate

controls ($p50^{Fl/Fl}$), whereas $p50^{Fl/Fl}$;VillinCre and $p50^{Fl/Fl}$ mice showed a similar number of tumors (Fig. 7B). These results demonstrate the role of myeloid-specific p50 in tumor promotion, fostering the analysis of its impact on CRC patients' outcome. To this aim, we assessed the nuclear expression of p50 in $CD68^+$ TAMs from stage II and III CRC patients (Supplementary Table S1). A direct correlation was observed between the percentage of $p50^+CD68^+$ TAMs within the tumor and those at the invasive front (Correlation coefficient (r)= 0,733161; r^2 = 0,537524). Such correlation was similar in stage II and stage III CRCs.

The percentage of nuclear $p50^+CD68^+$ TAMs at the invasive front (but not of those within the tumor) was significantly higher (two-tailed unpaired *t*-test, p=0.007) in patients with post-surgical progression (Fig. 7C, left and Supplementary Fig. S8B, left). Consistently, the higher density of $p50^+$ TAMs at the invasive front (but not of those within the tumor) was associated with a significantly worse patient outcome, assessed both as relapse (DFS, Log-rank test, p=0.0032) and as CRC-specific survival (CRC-SS, Log-rank test, p=0.0010) (Fig. 7C, center and right and Supplementary Fig. S8B, center and right).

Next, we investigated whether nuclear accumulation of p50 in peritumoral TAMs correlated with inhibition of M1-driven antitumor immunity. To this aim, we analyzed the expression of mRNAs coding for type 1 inflammatory genes (*IL12A, IL12B, CXCL9, CXCL10, IL21, TBX21*) in tumor tissues of stage II and III CRCs. We observed that the mRNA expression of most inflammatory genes was significantly correlated among themselves, with a clear inverse correlation between *IL12A* mRNA and the density of $p50^+CD68^+$ TAMs at the invasive front (Kendall's tau, -0.37; p=0.0072). In agreement, comparing M1/Th1 gene expression in groups of patients characterized by high and low numbers of $p50^+$ TAMs, we found an inverse correlation between the density of $p50^+$

TAMs and the expression of both the *IL12A* and *TBX21* genes (data cleaned by outliers passed D'Agostino & Pearson omnibus normality test and were analyzed by two-tailed *t*-test; Fig. 7D). We observed that the mRNA of *CXCL9*, *CXCL10* and *IL21* consistently tended to be lower in the group with a high number of $p50^+$ TAMs (Fig. 7D). Higher expression of the inflammatory genes *IL12A, TBX21, CXCL9, CXCL10* and *IL21* were associated with increased disease-free survival (DFS) and lower disease progression (Fig. 7E), as well as with improved CRC-SS (Fig. 7F). Our results indicate that the accumulation of p50 NF-κB in TAMs located at the invasive edge of CRC and conversely low levels of type I inflammation are associated with a worse clinical outcome.

Discussion

Following the recognition of infiltrating immune cells as determinants of tumor progression (41), the concept that robust adaptive immune responses in the tumor microenvironment can counteract CRC progression towards systemic dissemination, and, thus, positively affect patient outcome, has been exemplified by a prognostic immunoscore measuring the amount of T lymphocytes (14). Differently, the accumulation of TAMs, acting as orchestrator of cancer-related inflammation (4,16), is usually associated with an M2-polarized, tumor-promoting phenotype (36) and poor prognosis in most human tumors (17-19). However, TAMs' impact on CRC remains controversial. Here, we report that accumulation of $p50^+$ TAMs at the invasive margin negatively affected the outcome of patients with stage II/III CRC. A high number of $p50^+$ TAMs was associated with low expression of both *IL12A* and *TBX21* mRNA and, in general, with decreased expression of Th1/M1 genes. These findings support the concept that nuclear accumulation of p50 in TAMs restrains Th1/M1-dependent antitumor responses and mark a subgroup of TAMs with pro-tumor features in CRC that

may negatively affect outcome. Several evidences from our pre-clinical models also support the M2 relevance of the $p50^{+}$ TAMs.

Although the M1 to M2 switch of TAM functions has been largely debated (11,13,36,42), the molecular basis and clinical relevance of this dynamic reprogramming has been only partially elucidated. The results of our study, obtained using either the AOM/DSS or the Apc^{Min} mouse models, both of which develop multiple polyps (19,39), indicate that independent of the etiological trigger, the dynamic and p50-dependent inhibition of M1 polarization of macrophages is a crucial event for intestinal tumor growth. Our data indicate that p50 accumulation in tumors paralleled increased expression of a gene cluster (cluster 2) containing both M2-related (*Il10, Tgfb1, Ccl17, Ccl22*) and selected tumor promoting (*Tnf* and *Il23a*) genes. This dynamic, transcriptional transition appears to create tumor-promoting conditions by hampering the cytotoxic actions of the Th1/M1-polarized inflammatory and cytotoxic gene cluster 1.

Analysis of the leukocyte infiltrate in wt and p50-deficient tumor-bearing mice revealed a strong reduction of both TAMs and lamina propria macrophages. As gut macrophages are constantly replenished by bone marrow-derived monocytes (43), our results suggest that p50 is required for intestinal monocyte/macrophage turnover, suggesting additional roles of p50 in macrophage biology, which underlines the need of future studies to further dissect the role of p50 in myeloid cell biology and tumor development.

At steady state, NK, NKT, and T cells were similarly present in the lamina propria of wt and $p50^{-/-}$ mice, whereas they increased in both the adjacent healthy mucosa and tumor lesions of AOM/DSS-treated mice. In accordance with these findings, $p50^{-/-}$ tumors expressed higher type 1-specific chemokines (e.g. *Cxcl9, Cxcl10*), cytokines

(*Il12a, Il12b, Il27, Il21*), and effector molecules (*Ifng, Prf1, Gzmb, Fasl*). Although IL21 can support CRC by promoting Th17-driven inflammation (44-46), this cytokine can also elicit antitumor effects (47,48) by favoring the development, expansion, and cytotoxic activities of $CD8^+$ T cells, NKT and NK cells (49). Of relevance, increased *Il21* expression in $p50^{-/-}$ tumor-bearing mice did not correlate with enhanced expression of neither *Il17a* nor *Rorc2* (RORγt), but rather with increased genes expressed by cytotoxic lymphoid cells (e. g. *Ifng, Prf1, Gzmb, Fasl, Tbx21* (Tbet)) and frequency of IFNγ expressing $CD8^+$ and $CD4^+$ T cells. Hence, in line with previous reports (50), lack of p50 appears to selectively enhance the antitumor effects of IL21, without engaging pro-tumoral Th17-driven inflammation.

In response to gut microbial products, myeloid cells orchestrate tumor-promoting IL23 and IL17 responses (51). In particular, IL23 drives Th17 cells expansion and functions (52) and inhibits NK cell effector functions (53). Accordingly, the increased expression of IL23p19, occurring during the AOM-DSS–driven transition from colitis to tumor, was prevented in $p50^{-/-}$ CRC and $Apc^{Min}p50^{-/-}$ mice. Overall, our results identify a mechanism by which p50 NF-κB promotes CRC progression by limiting Th1/M1 antitumor functions. This event is paralleled by both decreased accumulation of effector NK, NKT, and T cells and specific antitumor immunity. Although ablation of p50 may also impair CRC cell survival in a cell autonomous manner (54), our conclusion is supported by the observation that depletion of $CD4^+$ and $CD8^+$ T lymphocytes abolished the resistance of p50-deficient mice to colitis-associated CRC and that adoptive transfer of wt TAMs rescued MC38 tumor growth in $p50^{-/-}$ mice. The expression of p50 NF-κB itself, like that of the related cytokines and chemokines, has clear prognostic implications and deserves proper assessment in large clinical studies. Although blocking the activity of negative regulators of the inflammatory response, including p50, may

potentially elicit adverse reactions (55), administration of type 1 immune stimulators, such as IL12 and CXCL10, could offset adverse effects and restore antitumor immunity.

Acknowledgments

We acknowledge Dr. Camilla Recordati within Fondazione Filarete, Milano and Dr. Vincenzo Arena Università Cattolica del Sacro Cuore, Roma for animal histopathology.

Authors' Contributions: C.P., A.S. designed research; C.P., A.I., F.M.C., L.C., G.C., F.G., F.P., S.T. C.C. performed research; C.P., A.I., F.M.C., L.C., G.C., F.G., P.B., S.V. analyzed data; F.B., E.T., E.H. generated NFKB1Fl/+ mice; L.L. analyzed data and critical revised the manuscript; C.P., A.S. wrote the paper.

REFERENCES

1. Rogler G. Chronic ulcerative colitis and colorectal cancer. Cancer letters **2014**;345(2):235-41 doi 10.1016/j.canlet.2013.07.032.
2. Quante M, Varga J, Wang TC, Greten FR. The gastrointestinal tumor microenvironment. Gastroenterology **2013**;145(1):63-78 doi 10.1053/j.gastro.2013.03.052.
3. Wang K, Karin M. Tumor-Elicited Inflammation and Colorectal Cancer. Advances in cancer research **2015**;128:173-96 doi 10.1016/bs.acr.2015.04.014.
4. Mantovani A, Allavena P, Sica A, Balkwill F. Cancer-related inflammation. Nature **2008**;454(7203):436-44 doi 10.1038/nature07205.
5. Ruffell B, Affara NI, Coussens LM. Differential macrophage programming in the tumor microenvironment. Trends in immunology **2012**;33(3):119-26 doi 10.1016/j.it.2011.12.001.
6. Porta C, Riboldi E, Ippolito A, Sica A. Molecular and epigenetic basis of macrophage polarized activation. Seminars in immunology **2015**;27(4):237-48 doi 10.1016/j.smim.2015.10.003.
7. Schwitalla S, Ziegler PK, Horst D, Becker V, Kerle I, Begus-Nahrmann Y, *et al.* Loss of p53 in enterocytes generates an inflammatory microenvironment enabling invasion and lymph node metastasis of carcinogen-induced colorectal tumors. Cancer cell **2013**;23(1):93-106 doi 10.1016/j.ccr.2012.11.014.
8. Greten FR, Eckmann L, Greten TF, Park JM, Li ZW, Egan LJ, *et al.* IKKbeta links inflammation and tumorigenesis in a mouse model of colitis-associated cancer. Cell **2004**;118(3):285-96 doi 10.1016/j.cell.2004.07.013.

9. Grivennikov S, Karin E, Terzic J, Mucida D, Yu GY, Vallabhapurapu S, *et al.* IL-6 and Stat3 are required for survival of intestinal epithelial cells and development of colitis-associated cancer. Cancer cell **2009**;15(2):103-13 doi 10.1016/j.ccr.2009.01.001.
10. Bollrath J, Phesse TJ, von Burstin VA, Putoczki T, Bennecke M, Bateman T, *et al.* gp130-mediated Stat3 activation in enterocytes regulates cell survival and cell-cycle progression during colitis-associated tumorigenesis. Cancer cell **2009**;15(2):91-102 doi 10.1016/j.ccr.2009.01.002.
11. Goktuna SI, Canli O, Bollrath J, Fingerle AA, Horst D, Diamanti MA, *et al.* IKKalpha promotes intestinal tumorigenesis by limiting recruitment of M1-like polarized myeloid cells. Cell reports **2014**;7(6):1914-25 doi 10.1016/j.celrep.2014.05.006.
12. Pasparakis M. Regulation of tissue homeostasis by NF-kappaB signalling: implications for inflammatory diseases. Nature reviews Immunology **2009**;9(11):778-88 doi 10.1038/nri2655.
13. Mantovani A, Sica A. Macrophages, innate immunity and cancer: balance, tolerance, and diversity. Current opinion in immunology **2010**;22(2):231-7 doi 10.1016/j.coi.2010.01.009.
14. Galon J, Mlecnik B, Bindea G, Angell HK, Berger A, Lagorce C, *et al.* Towards the introduction of the 'Immunoscore' in the classification of malignant tumours. The Journal of pathology **2014**;232(2):199-209 doi 10.1002/path.4287.
15. Laghi L, Bianchi P, Miranda E, Balladore E, Pacetti V, Grizzi F, *et al.* CD3+ cells at the invasive margin of deeply invading (pT3-T4) colorectal cancer and risk of post-surgical metastasis: a longitudinal study. The Lancet Oncology **2009**;10(9):877-84 doi 10.1016/S1470-2045(09)70186-X.
16. Qian BZ, Pollard JW. Macrophage diversity enhances tumor progression and metastasis. Cell **2010**;141(1):39-51 doi 10.1016/j.cell.2010.03.014.
17. Bingle L, Brown NJ, Lewis CE. The role of tumour-associated macrophages in tumour progression: implications for new anticancer therapies. The Journal of pathology **2002**;196(3):254-65 doi 10.1002/path.1027.
18. Steidl C, Lee T, Shah SP, Farinha P, Han G, Nayar T, *et al.* Tumor-associated macrophages and survival in classic Hodgkin's lymphoma. The New England journal of medicine **2010**;362(10):875-85 doi 10.1056/NEJMoa0905680.
19. Dannenmann SR, Thielicke J, Stockli M, Matter C, von Boehmer L, Cecconi V, *et al.* Tumor-associated macrophages subvert T-cell function and correlate with reduced survival in clear cell renal cell carcinoma. Oncoimmunology **2013**;2(3):e23562 doi 10.4161/onci.23562.
20. Zhang QW, Liu L, Gong CY, Shi HS, Zeng YH, Wang XZ, *et al.* Prognostic significance of tumor-associated macrophages in solid tumor: a meta-analysis of the literature. PloS one **2012**;7(12):e50946 doi 10.1371/journal.pone.0050946.
21. Erreni M, Mantovani A, Allavena P. Tumor-associated Macrophages (TAM) and Inflammation in Colorectal Cancer. Cancer microenvironment : official journal of the International Cancer Microenvironment Society **2011**;4(2):141-54 doi 10.1007/s12307-010-0052-5.
22. Braster R, Bogels M, Beelen RH, van Egmond M. The delicate balance of macrophages in colorectal cancer; their role in tumour development and therapeutic potential. Immunobiology **2015** doi 10.1016/j.imbio.2015.08.011.
23. Norton SE, Ward-Hartstonge KA, Taylor ES, Kemp RA. Immune cell interplay in colorectal cancer prognosis. World journal of gastrointestinal oncology **2015**;7(10):221-32 doi 10.4251/wjgo.v7.i10.221.

24. Kang JC, Chen JS, Lee CH, Chang JJ, Shieh YS. Intratumoral macrophage counts correlate with tumor progression in colorectal cancer. Journal of surgical oncology **2010**;102(3):242-8 doi 10.1002/jso.21617.
25. Forssell J, Oberg A, Henriksson ML, Stenling R, Jung A, Palmqvist R. High macrophage infiltration along the tumor front correlates with improved survival in colon cancer. Clinical cancer research : an official journal of the American Association for Cancer Research **2007**;13(5):1472-9 doi 10.1158/1078-0432.CCR-06-2073.
26. Wang W, Li X, Zheng D, Zhang D, Peng X, Zhang X*, et al.* Dynamic changes and functions of macrophages and M1/M2 subpopulations during ulcerative colitis-associated carcinogenesis in an AOM/DSS mouse model. Molecular medicine reports **2015**;11(4):2397-406 doi 10.3892/mmr.2014.3018.
27. Edin S, Wikberg ML, Dahlin AM, Rutegard J, Oberg A, Oldenborg PA*, et al.* The distribution of macrophages with a M1 or M2 phenotype in relation to prognosis and the molecular characteristics of colorectal cancer. PloS one **2012**;7(10):e47045 doi 10.1371/journal.pone.0047045.
28. Saccani A, Schioppa T, Porta C, Biswas SK, Nebuloni M, Vago L*, et al.* p50 nuclear factor-kappaB overexpression in tumor-associated macrophages inhibits M1 inflammatory responses and antitumor resistance. Cancer research **2006**;66(23):11432-40 doi 10.1158/0008-5472.CAN-06-1867.
29. Porta C, Rimoldi M, Raes G, Brys L, Ghezzi P, Di Liberto D*, et al.* Tolerance and M2 (alternative) macrophage polarization are related processes orchestrated by p50 nuclear factor kappaB. Proceedings of the National Academy of Sciences of the United States of America **2009**;106(35):14978-83 doi 10.1073/pnas.0809784106.
30. Miranda E, Bianchi P, Destro A, Morenghi E, Malesci A, Santoro A*, et al.* Genetic and epigenetic alterations in primary colorectal cancers and related lymph node and liver metastases. Cancer **2013**;119(2):266-76 doi 10.1002/cncr.27722.
31. Okayasu I, Ohkusa T, Kajiura K, Kanno J, Sakamoto S. Promotion of colorectal neoplasia in experimental murine ulcerative colitis. Gut **1996**;39(1):87-92.
32. Cooper HS, Murthy SN, Shah RS, Sedergran DJ. Clinicopathologic study of dextran sulfate sodium experimental murine colitis. Lab Invest **1993**;69(2):238-49.
33. Suzuki R, Kohno H, Sugie S, Tanaka T. Dose-dependent promoting effect of dextran sodium sulfate on mouse colon carcinogenesis initiated with azoxymethane. Histol Histopathol **2005**;20(2):483-92 doi 10.14670/HH-20.483.
34. Johnston RJ, Poholek AC, DiToro D, Yusuf I, Eto D, Barnett B*, et al.* Bcl6 and Blimp-1 are reciprocal and antagonistic regulators of T follicular helper cell differentiation. Science **2009**;325(5943):1006-10 doi 10.1126/science.1175870.
35. Galon J, Costes A, Sanchez-Cabo F, Kirilovsky A, Mlecnik B, Lagorce-Pages C*, et al.* Type, density, and location of immune cells within human colorectal tumors predict clinical outcome. Science **2006**;313(5795):1960-4 doi 10.1126/science.1129139.
36. Sica A, Mantovani A. Macrophage plasticity and polarization: in vivo veritas. The Journal of clinical investigation **2012**;122(3):787-95 doi 10.1172/JCI59643.
37. Salcedo R, Worschech A, Cardone M, Jones Y, Gyulai Z, Dai RM*, et al.* MyD88-mediated signaling prevents development of adenocarcinomas of the colon: role of interleukin 18. The Journal of experimental medicine **2010**;207(8):1625-36 doi 10.1084/jem.20100199.

38. Rakoff-Nahoum S, Medzhitov R. Regulation of spontaneous intestinal tumorigenesis through the adaptor protein MyD88. Science **2007**;317(5834):124-7 doi 10.1126/science.1140488.
39. Moser AR, Pitot HC, Dove WF. A dominant mutation that predisposes to multiple intestinal neoplasia in the mouse. Science **1990**;247(4940):322-4.
40. Ries CH, Cannarile MA, Hoves S, Benz J, Wartha K, Runza V*, et al.* Targeting tumor-associated macrophages with anti-CSF-1R antibody reveals a strategy for cancer therapy. Cancer cell **2014**;25(6):846-59 doi 10.1016/j.ccr.2014.05.016.
41. Balkwill F, Mantovani A. Inflammation and cancer: back to Virchow? Lancet **2001**;357(9255):539-45 doi 10.1016/S0140-6736(00)04046-0.
42. Hefetz-Sela S, Stein I, Klieger Y, Porat R, Sade-Feldman M, Zreik F*, et al.* Acquisition of an immunosuppressive protumorigenic macrophage phenotype depending on c-Jun phosphorylation. Proceedings of the National Academy of Sciences of the United States of America **2014**;111(49):17582-7 doi 10.1073/pnas.1409700111.
43. Bain CC, Scott CL, Uronen-Hansson H, Gudjonsson S, Jansson O, Grip O*, et al.* Resident and pro-inflammatory macrophages in the colon represent alternative context-dependent fates of the same Ly6Chi monocyte precursors. Mucosal immunology **2013**;6(3):498-510 doi 10.1038/mi.2012.89.
44. Jauch D, Martin M, Schiechl G, Kesselring R, Schlitt HJ, Geissler EK*, et al.* Interleukin 21 controls tumour growth and tumour immunosurveillance in colitis-associated tumorigenesis in mice. Gut **2011**;60(12):1678-86 doi 10.1136/gutjnl-2011-300612.
45. Stolfi C, Rizzo A, Franze E, Rotondi A, Fantini MC, Sarra M*, et al.* Involvement of interleukin-21 in the regulation of colitis-associated colon cancer. The Journal of experimental medicine **2011**;208(11):2279-90 doi 10.1084/jem.20111106.
46. De Simone V, Ronchetti G, Franze E, Colantoni A, Ortenzi A, Fantini MC*, et al.* Interleukin-21 sustains inflammatory signals that contribute to sporadic colon tumorigenesis. Oncotarget **2015**;6(12):9908-23 doi 10.18632/oncotarget.3532.
47. Ugai S, Shimozato O, Kawamura K, Wang YQ, Yamaguchi T, Saisho H*, et al.* Expression of the interleukin-21 gene in murine colon carcinoma cells generates systemic immunity in the inoculated hosts. Cancer gene therapy **2003**;10(3):187-92 doi 10.1038/sj.cgt.7700552.
48. Bindea G, Mlecnik B, Tosolini M, Kirilovsky A, Waldner M, Obenauf AC*, et al.* Spatiotemporal dynamics of intratumoral immune cells reveal the immune landscape in human cancer. Immunity **2013**;39(4):782-95 doi 10.1016/j.immuni.2013.10.003.
49. Spolski R, Leonard WJ. Interleukin-21: a double-edged sword with therapeutic potential. Nature reviews Drug discovery **2014**;13(5):379-95 doi 10.1038/nrd4296.
50. Larghi P, Porta C, Riboldi E, Totaro MG, Carraro L, Orabona C*, et al.* The p50 subunit of NF-kappaB orchestrates dendritic cell lifespan and activation of adaptive immunity. PloS one **2012**;7(9):e45279 doi 10.1371/journal.pone.0045279.
51. Grivennikov SI, Wang K, Mucida D, Stewart CA, Schnabl B, Jauch D*, et al.* Adenoma-linked barrier defects and microbial products drive IL-23/IL-17-mediated tumour growth. Nature **2012**;491(7423):254-8 doi 10.1038/nature11465.

52. Langrish CL, Chen Y, Blumenschein WM, Mattson J, Basham B, Sedgwick JD*, et al.* IL-23 drives a pathogenic T cell population that induces autoimmune inflammation. The Journal of experimental medicine **2005**;201(2):233-40 doi 10.1084/jem.20041257.
53. Teng MW, Andrews DM, McLaughlin N, von Scheidt B, Ngiow SF, Moller A*, et al.* IL-23 suppresses innate immune response independently of IL-17A during carcinogenesis and metastasis. Proceedings of the National Academy of Sciences of the United States of America **2010**;107(18):8328-33 doi 10.1073/pnas.1003251107.
54. Southern SL, Collard TJ, Urban BC, Skeen VR, Smartt HJ, Hague A*, et al.* BAG-1 interacts with the p50-p50 homodimeric NF-kappaB complex: implications for colorectal carcinogenesis. Oncogene **2012**;31(22):2761-72 doi 10.1038/onc.2011.452.
55. Erdman S, Fox JG, Dangler CA, Feldman D, Horwitz BH. Typhlocolitis in NF-kappa B-deficient mice. J Immunol **2001**;166(3):1443-7.

FIGURE LEGENDS

Figure 1: Association between distinct inflammatory gene clusters and clinical outcome. A, Expression of selected inflammatory genes was analyzed in total RNA extracted from colons of mice with colitis (after the first cycle of DSS administration), tumors, and adjacent healthy tissue at the end of the AOM/DSS experiment. Total RNA from colon of untreated mice was used as control. Normalized qPCR results shown as fold increase over control. Cluster 1: genes similarly upregulated in colitis and tumor stages. Cluster 2: genes reaching the maximum peak of expression at the tumor stage. Box: the 25th–75th percentiles; Line: the median; Whiskers: range. **P*≤0.05 by two-tailed Kruskal-Wallis with Dunn's correction for multiple comparisons. Control (-): white boxes, N=4 different mice; Colitis: green boxes, N=9 different mice; Tumor: blue boxes, N= 13 different mice; Healthy (AOM/DSS): gray boxes, N=5 different mice. **B,** immunofluorescence of nuclear p50 (white) and p65 (red) in colonic and TAMs ($F4/80^+$ cells; green). N=326 single $F4/80^+$ cells analyzed from 7 total images of colons from 2

untreated wt mice; N=1314 single F4/80$^+$ cells analyzed from 52 total images of 16 tumors from 5 AOM/DSS-treated wt mice. Error bars, SEM. *P<0.05 by two-tailed unpaired t test. Representative images shown. Scale bars: 10 μm.

Figure 2: p50 NF-κB promotes CAC by hampering M1/Th1 inflammation. To induce CAC, mice were treated with AOM and DSS. **A,** Top: Body weight monitored every 2-3 days during the experimental period (multi t-test, starting from day 10 *FDR<0.05; N=16). Bottom: Colon length measured at the time of mice sacrifice (day 100). Data shown are mean±SEM of different mice from two independent experiments. ***P<0.001 by two-tailed Mann Whitney test. Untreated wt: N=6; Untreated p50$^{-/-}$: N=6; AOM/DSS-treated wt: N=17; AOM/DSS-treated p50$^{-/-}$: N=12. Center: Ulceration and degree of inflammation (colitis score) analyzed on colon swiss roll sections by H&E. Data shown are mean±SEM of different mice from two independent experiments. *P<0.05 by two-tailed Mann Whitney test. wt: N=11; p50$^{-/-}$: N=9. **B,** Colons were longitudinally opened and polyps were counted. Data shown are mean±SEM of different mice from two independent experiments. ***P<0.001 by two-tailed Mann Whitney test. wt: N=11; p50$^{-/-}$: N=9. Representative images are shown. The total number and the size of tumors were counted and tumor burden was calculated for each animal. Data shown are mean±SEM of different mice or tumors from two independent experiments. *P<0.05, ***P<0.001 by two-tailed Mann Whitney test. N=11 different wt mice; N=9 different p50$^{-/-}$ mice; N=52 wt tumors; N=9 p50$^{-/-}$ tumors). Representative images are shown. Scale bars: 1000 μm. **C,** Top: Total RNA from tumors of AOM/DSS-treated wt and p50$^{-/-}$ mice analyzed for the expression of the genes belonging to clusters 1 and 2, and Bottom: additional Th1/M1 genes. Results are expressed as fold induction over wt tumor expression. Data shown are mean±SEM of different mice from two independent experiments. *P<0.05 by one-

tailed Mann Whitney test N=13 wt mice; N=15 $p50^{-/-}$ mice. **D,** Top: FACS analysis of CRC lesions for selective M1 gene products in TAMs ($CD11b^{+}F4/80^{+}$ cells) and Bottom: the frequency of IFNγ-expressing T cells. Intracellular expression of cytokines (IL12, TNFα, IFNγ) was measured upon 3h of stimulation with 50 ng/mL PMA and 1 μg/mL ionomycin in presence of 5 μg/mL Brefeldin A. Data shown are mean±SEM. **P*<0.05, ***P*<0.01 by two-tailed *t* test. N=6 wt mice; N=5 $p50^{-/-}$ mice. Center: Representative FACS histograms of M1 markers are shown.

Figure 3: Administration of M1 cytokines inhibits CAC development. A, Treatment regimen with IL12 and CXCL10 during CAC induction. **B,** Body weight loss during the treatment. *FDR<0.05 by multi t-test of treated versus vehicle. N=10 vehicle treated mice; N= 7 IL12 treated mice; N=8 CXCL10 treated mice. **C,** Colon length of mice treated with vehicle, IL12, or CXCL10, and **D,** analysis of tumor development (number of polyps) was performed at day 80 on longitudinally opened colons. Representative images are shown. Data shown are mean±SEM. **P*<0.05 by one-tailed Mann Whitney test. N=5 vehicle treated mice; N=6 IL12 treated mice; N=6 CXCL10 treated mice.

Figure 4: Lack of p50 in Apc^{Min} mice inhibits spontaneous intestinal tumor development. A, Histological analysis of small gut and colons harvested from Apc^{Min} and $Apc^{Min}p50^{-/-}$ mice at 12 or 18 weeks of age. Number and size of tumors was monitored, and tumor burden calculated for each mouse. Data shown are mean±SEM of different mice or tumors. **P*<0.05, ***P*<0.01, ****P*<0.001 by two-tailed_Mann Whitney test. N=7 Apc^{Min} mice 12 weeks old; N=8 $Apc^{Min}p50^{-/-}$ mice 12 weeks old; N=13 Apc^{Min} mice 18 weeks old; N=15 $Apc^{Min}p50^{-/-}$ mice 18 weeks old; N=76 tumors from Apc^{Min} mice 12 weeks old; N=39 tumors from $Apc^{Min}p50^{-/-}$ mice 12 weeks old; N=155 tumors

from Apc^{Min} mice 18 weeks old; N=133 tumors from $Apc^{Min}p50^{-/-}$ mice 18 weeks old). **B,** Survival time of Apc^{Min} and $Apc^{Min}p50^{-/-}$ mice. ***P<0.0001 by log-rank Mantel-Cox test. N=54 Apc^{Min} mice; N=26 $Apc^{Min}p50^{-/-}$ mice. **C-D,** expression of gene clusters 1 and 2, and additional Th1/M1 genes in CRC lesions from Apc^{Min} mice vs. **C,** the adjacent healthy colonic mucosa and **D,** CRC lesions from $Apc^{Min}p50^{-/-}$ mice. Data shown are mean±SEM. *P<0.05 by one-tailed, Mann Whitney test. N=6 Apc^{Min} mice; N=6 $Apc^{Min}p50^{-/-}$ mice.

Figure 5: Modulation of gut-associated leukocyte populations by p50 NF-κB. A, Formalin-fixed and paraffin-embedded colons from AOM/DSS-treated and untreated mice (wt and $p50^{-/-}$) were evaluated for the number of macrophages ($F4/80^+$), monocytes ($Ly6C^+$), neutrophils ($Ly6G^+$), and T lymphocytes ($CD3^+$) by immunohistochemistry. *P<0.05, **P<0.01, ***P<0.001 one-tailed Mann Whitney test of wt (N=5) versus $p50^{-/-}$ (N=4) mice. **B,** Immunofluorescence analysis of frozen colonic samples were performed to evaluate NK ($CD3^-NKp46^+$) and NKT ($CD3^+NKp46^+$) cells. Data shown are mean±SEM of different tumors (wt N=15; $p50^{-/-}$ N=5) or fields (wt N=23; $p50^{-/-}$ N=23) of different mice. *P<0.05, **P<0.01 one-tailed Mann Whitney test of wt (N=6) versus $p50^{-/-}$ (N=3) mice. **C,** FACS analysis of CRC lesions for the frequency of the depicted immune cell populations. Data shown are mean±SEM of different mice. **P<0.01, ***P<0.001 two-tailed t-test. N=4 wt mice; N=4 $p50^{-/-}$ mice. **D**, Transcripts of genes encoding for markers of different leukocyte populations from healthy colons and tumors of untreated and AOM/DSS-treated mice. Results are shown as fold induction over healthy untreated wt mice. Data shown are mean±SEM. *P<0.05 by one-tailed Mann Whitney test. N=4 untreated wt mice; N=4 untreated $p50^{-/-}$ mice; N=5 AOM/DSS-treated wt mice; N=6 AOM/DSS-treated $p50^{-/-}$ mice). **E,** T cells were depleted from wt and $p50^{-/-}$ mice during the entire experimental period by i.p. injections of anti-CD4 (α-

CD4) and anti-CD8 (α-CD8). Control mice received vehicle (-) only. Tumor development was evaluated. Representative images of longitudinally opened colons at day 80 are shown. Data shown are mean±SEM. *P<0.05 two-tailed Kruskal-Wallis test N= 11 vehicle-treated wt mice; N= 10 vehicle-treated p50$^{-/-}$ mice; N= 10 anti-CD4/CD8-treated wt mice; N= 7 anti-CD4/CD8-treated p50$^{-/-}$ mice).

Figure 6: Lack of p50 increases apoptosis of both colonic epithelial and tumor cells after AOM/DSS administration. A, Activated cleaved caspase-3 in colon sections from AOM/DSS-treated and untreated mice by immunohistochemistry and digital image analysis. Representative images are shown. Data shown are mean±SEM of different fields. Scale bars are 20 μm. *P<0.05, **P<0.01 by one-tailed Mann Whitney test. N= 4 fields from 1 untreated wt mice; N= 4 fields from 1 untreated p50$^{-/-}$ mice; N=16 total tumor fields and N=14 total non-tumor fields from 5 different AOM/DSS-treated wt mice; N=8 total tumor fields and N=14 total non-tumor fields from 3 different AOM/DSS-treated p50$^{-/-}$ mice. **B,** Transcripts of survival genes were evaluated in total RNA isolated from colon and tumor lesions of untreated and AOM/DSS-treated mice. Normalized qPCR results are shown as fold induction over healthy untreated wt mice. Data shown are mean±SEM. *P<0.05 by one-tailed Mann Whitney test. N=2 untreated wt mice; N=2 untreated p50$^{-/-}$ mice; N=5 AOM/DSS-treatred wt mice; N=6 AOM/DSS-treated p50$^{-/-}$ mice.

Figure 7: Correlation between the number of p50 NF-κB^{+} TAMs and the clinical response of CRC patients. A, Histological analysis of colons from AOM/DSS-treated chimeric mice (p50$^{-/-}$ BM in wt recipients, N= 6 and wt BM in p50$^{-/-}$ recipients, N=7) with respect to control mice (N=14 lethally irradiated wt mice reconstituted with wt BM). *P<0.05 by one-tailed Mann Whitney test**. B,** Analysis of CRC lesions in AOM/DSS-

treated $p50^{Fl/Fl}$ (N=6) and $p50^{Fl/Fl}$;Lyz2Cre (N=7)(top) and $p50^{Fl/Fl}$ (N=6); $p50^{Fl/Fl}$;VillinCre (N=6) (bottom) mice. Data shown are mean±SEM. *P≤0.05 by one-tailed Mann Whitney test. **C,** Immunofluorescence of nuclear $p50^+$ TAMs ($CD68^+$ cells) in CRC lesions from 26 CRC patients, stage II and III. Left, analysis of the density of TAM with $p50^+$ nuclei at the invasive margin in relation with disease recurrence within 4 years from surgery. Two-tailed *t* test; **P<0.01. Center and right, the Kaplan-Meier analysis shows both disease-free survival (DFS) and CRC-specific survival (CRC-SS) of CRC patients, in relation to high (N=10; >mean; black line) or low (N=16; <mean; gray line) number of $p50^+$TAMs at the invasive margin. *P* values calculated by log-rank Mantel-Cox test; P<0.05 considered significant. **D,** Expression of selected type I inflammatory genes in total RNA obtained from 26 CRC patients (stage II and III CRC) in relation to high (>mean; black dots) or low (<mean; gray squares) number of $p50^+$TAMs located at the invasive margin. Data cleaned by outliers passed D'Agostino & Pearson omnibus normality test and analyzed by two-tailed t-test; *P<0.05, **P<0.01. **E-F,** Expression of selected type 1 inflammatory genes in total RNA from 47 stage II and III human CRC specimens. Results are normalized over the housekeeping gene β-actin. For each gene transcript, cut–off value was extrapolated by ROC curve analysis (*IL12A* $4.28x10^{-5}$; *IL12B* $7.88x10^{-5}$; *TBX21* $3.35x10^{-4}$; *CXCL9* $3.72x10^{-3}$; *CXCL10* $8.32x10^{-3}$; *IL21* $1.13x10^{-4}$). The Kaplan-Meier curves show **E,** DFS and **F,** CRC-SS of CRC patients in relation with the expression of the selected type 1 inflammatory genes in tumor samples. Black line: low gene transcripts (<cut-off value; *IL12A* N=18; *IL12B* N=37; *TBX21* N=32; *CXCL9* N=26; *CXCL10* N=29; *IL21* N=25); Gray line: high gene transcripts (>cut-off value; *IL12A* N=29; *IL12B* N=10; *TBX21* N=15; *CXCL9* N=21; *CXCL10* N=18; *IL21* N=22). *P* values were calculated by log-rank Mantel-Cox test; P<0.05 considered significant.

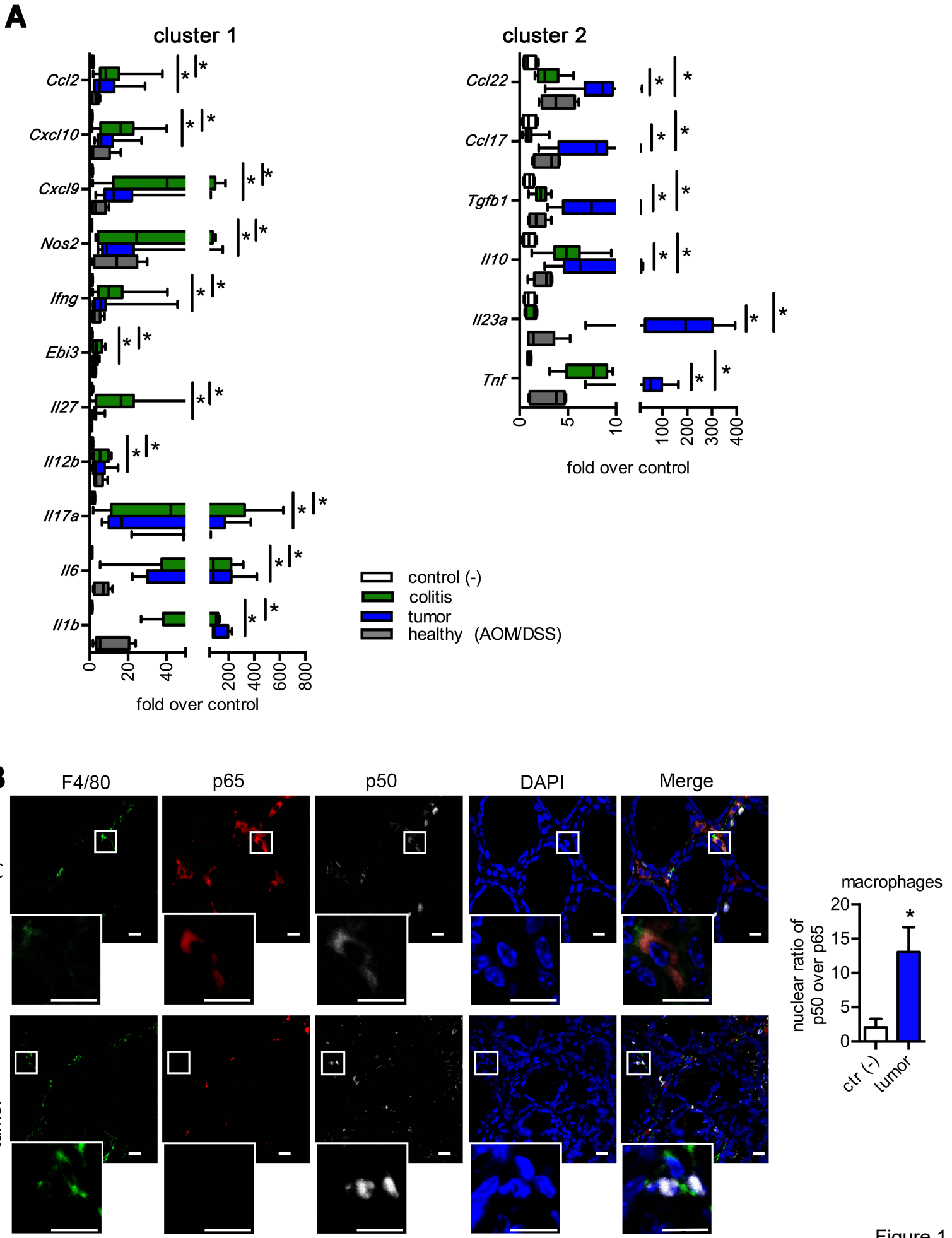

Figure 1

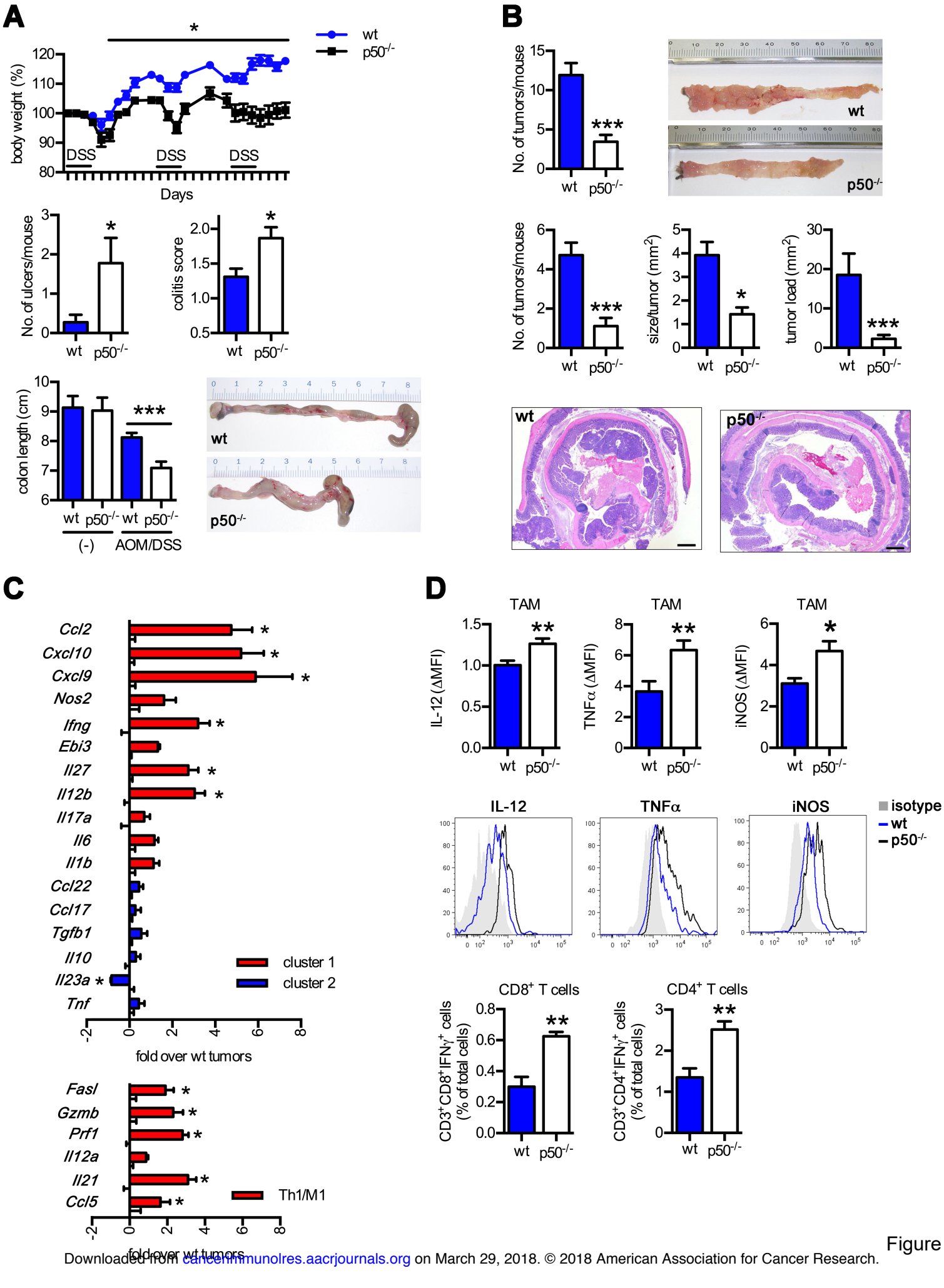

Figure 2

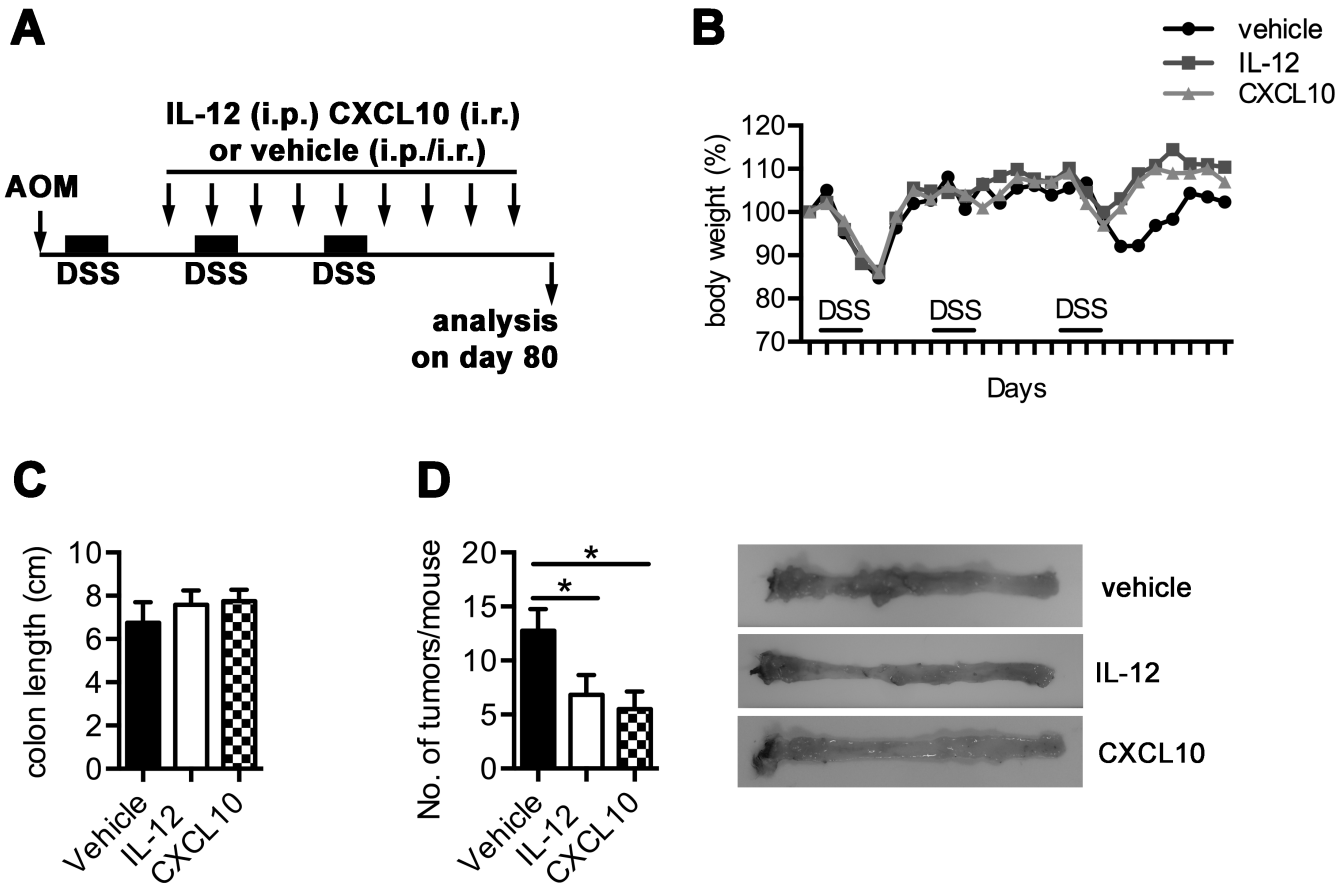

Figure 3

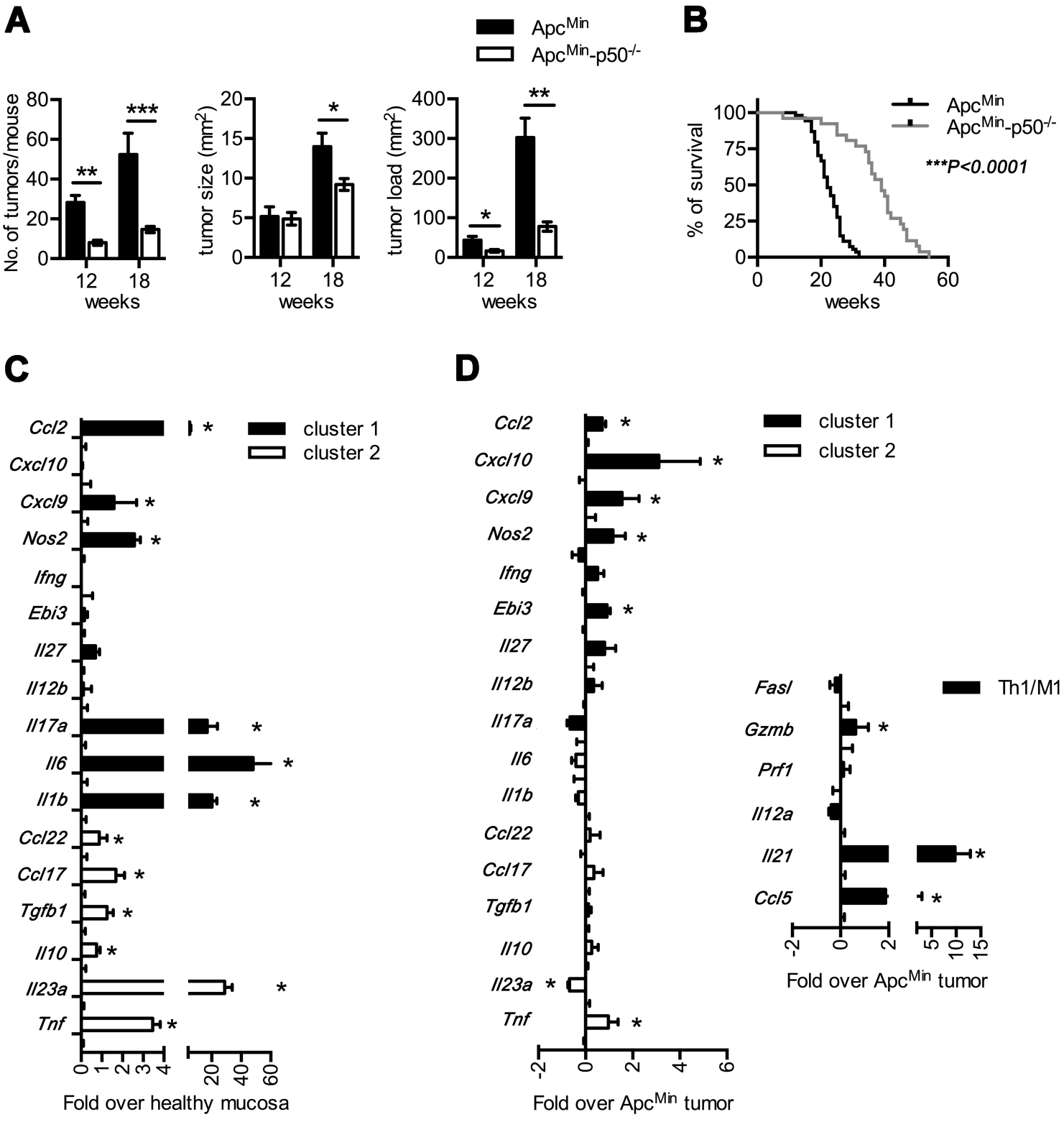

Figure 4

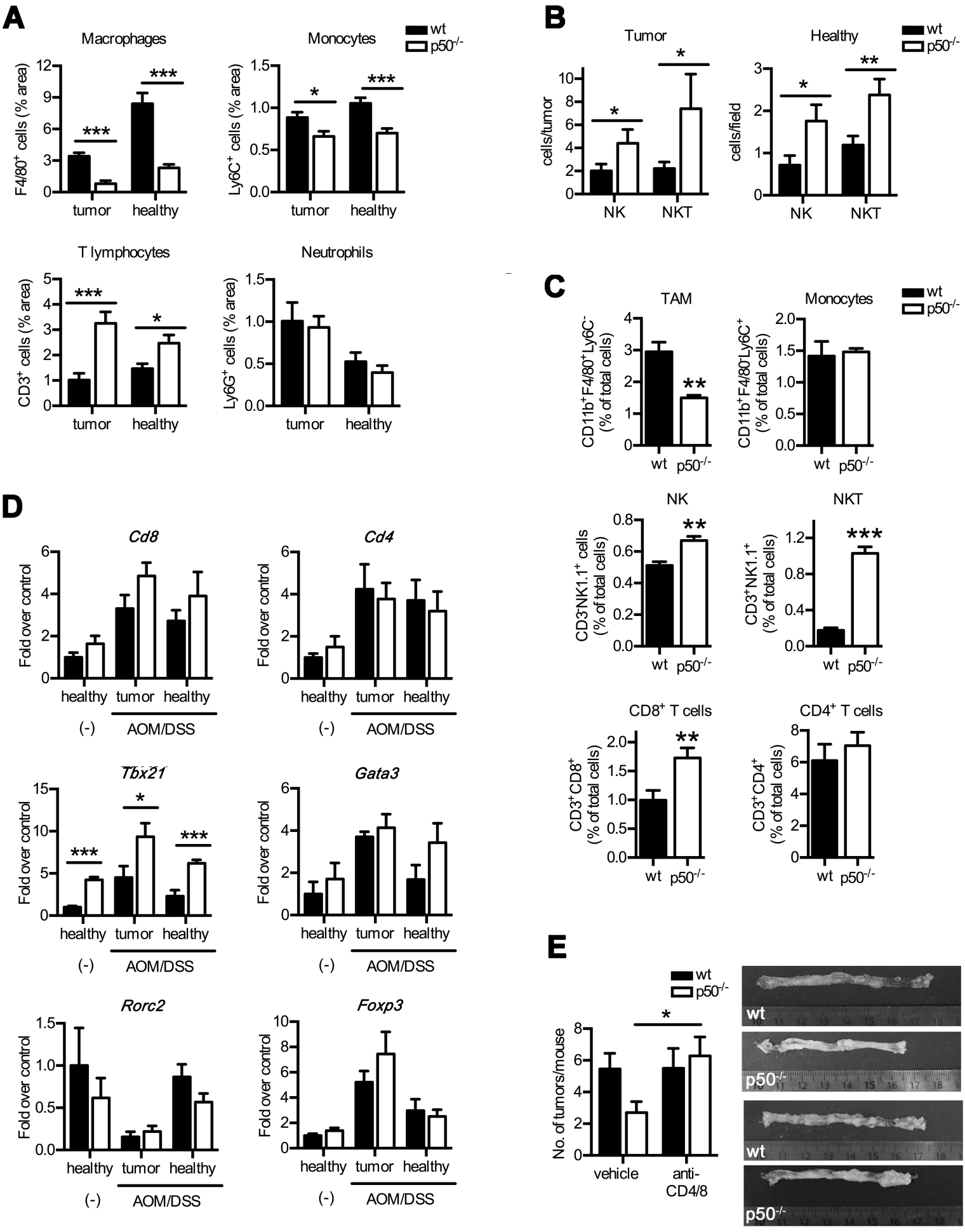

Figure 5

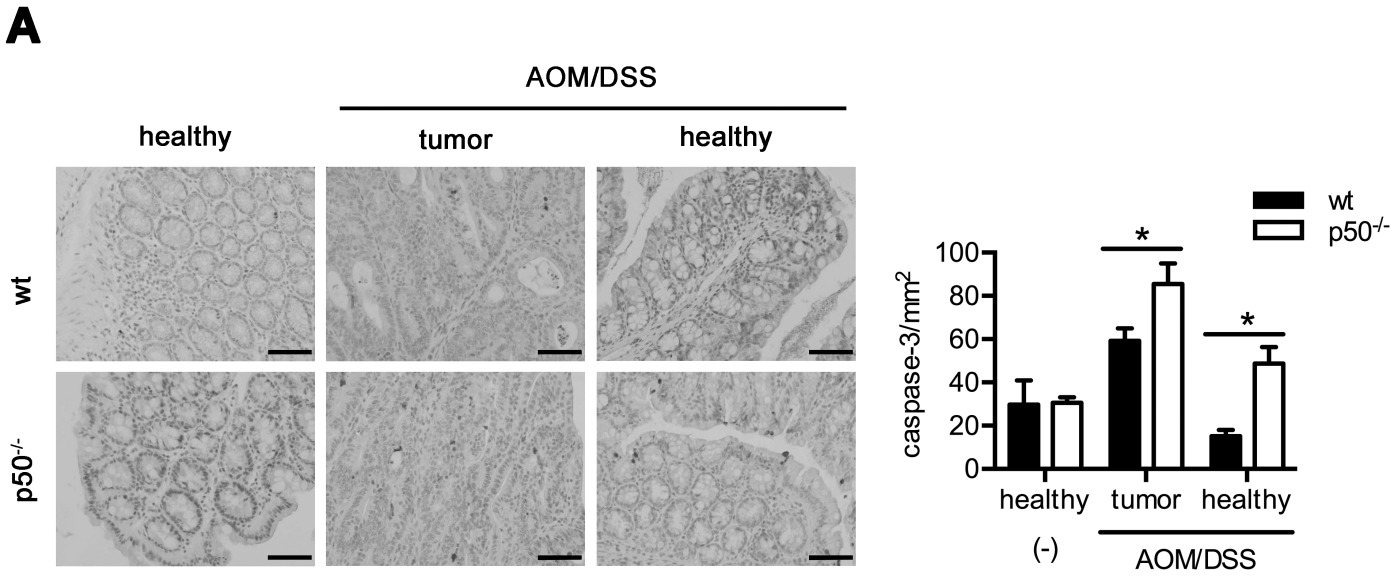

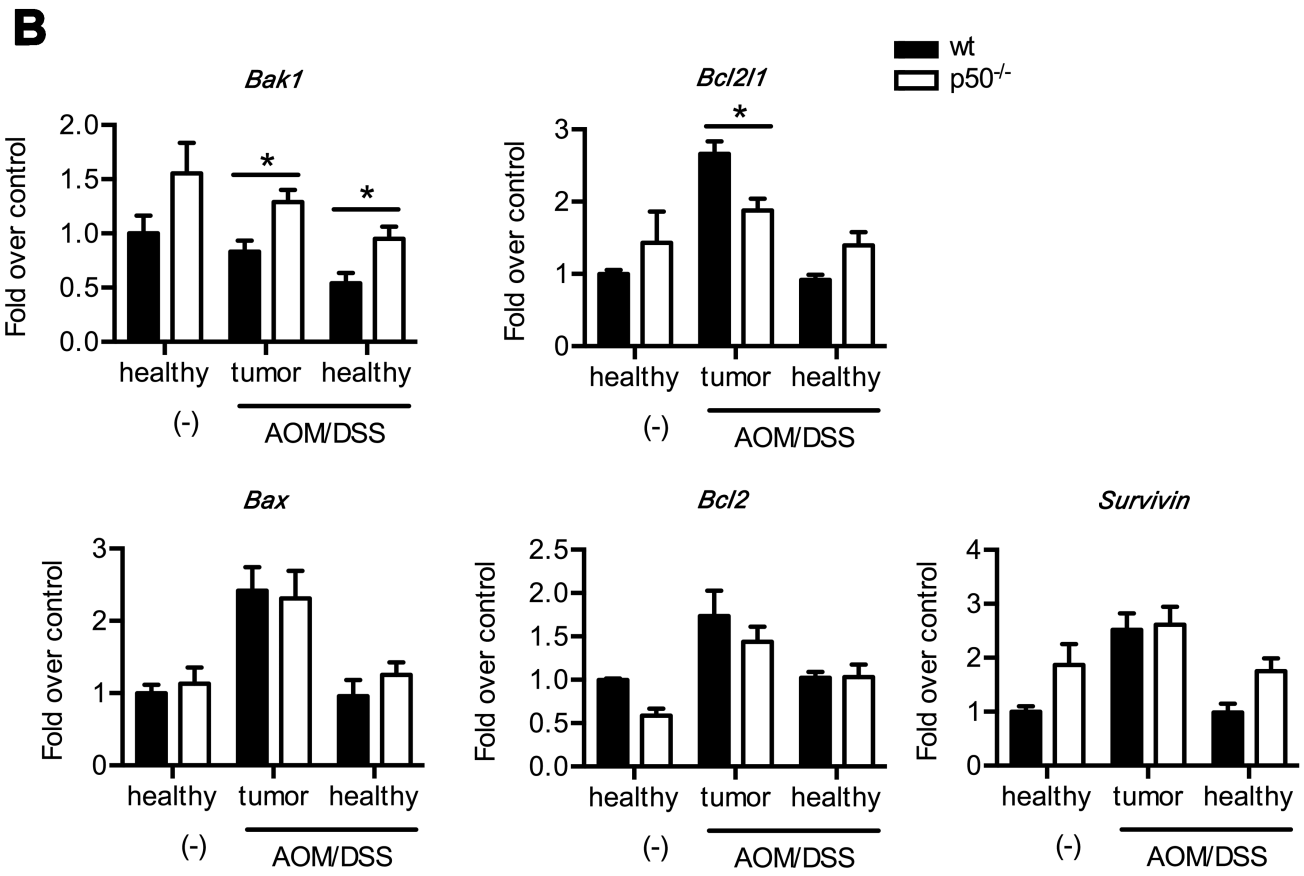

Figure 6

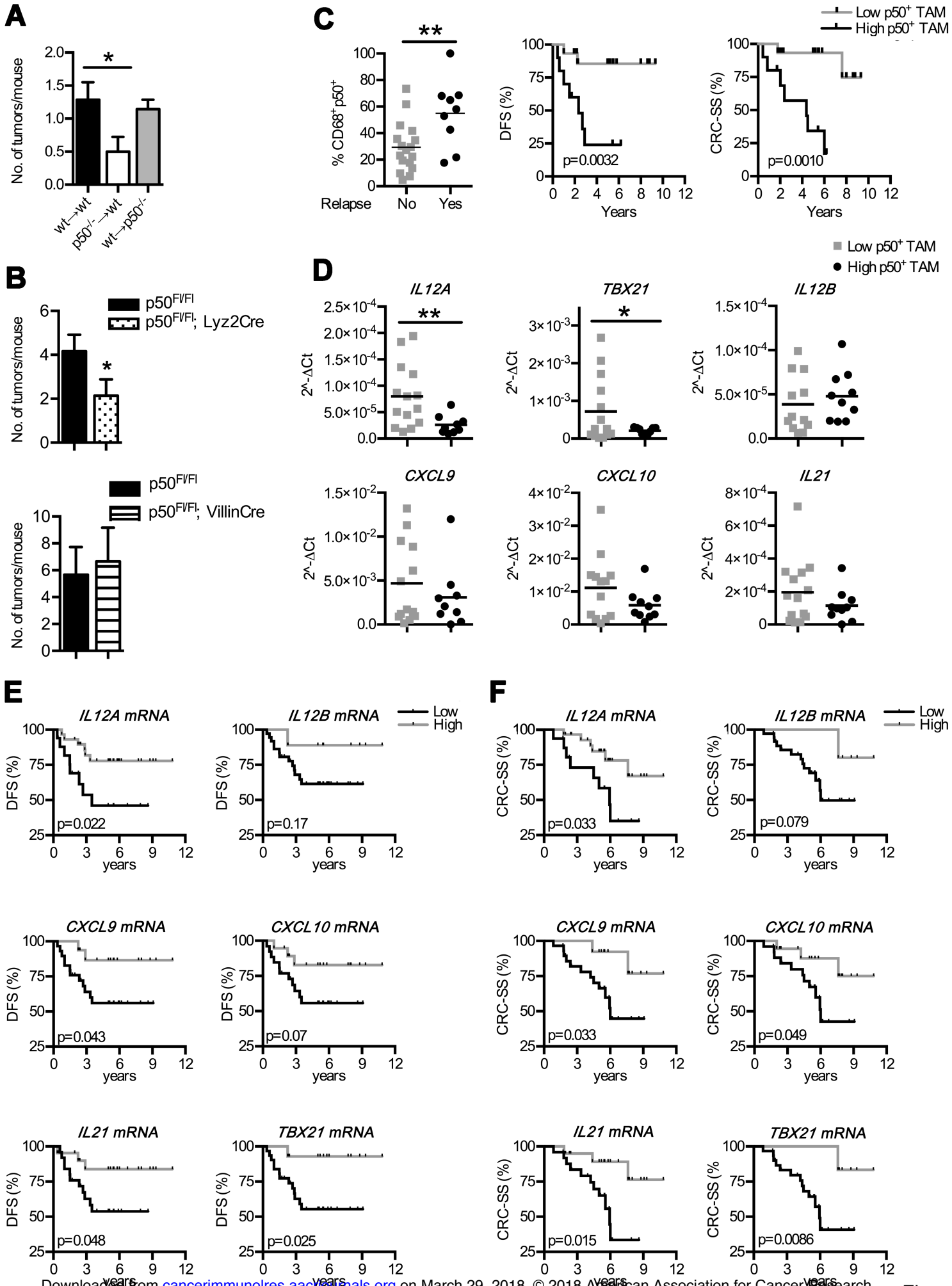

Figure 7